Iranian (Iranica) Journal of Energy & Environment
Journal Homepage: wwwijeenet
IJEE an official peer review journal of Babol Noshirvani University of Technology, ISSN:2079-2115

Effective Removal of Heavy Metal Using Cellulose Nanocomposite Adsorbents: Response Surface Methodology

A. Alipour[1], S. Zarinabadi[2]*, A. Azimi[1], M. Mirzaei[1]

[1] *Department of Chemical Engineering, Mahshahr Branch, Islamic Azad University, Mahshahr, Iran*
[2] *Department of Engineering, Ahvaz Branch, Islamic Azad University, Ahvaz, Iran*

P A P E R I N F O

Paper history:
Received 02 April 2022
Accepted in revised form 03 May 2022

Keywords:
Cellulose
Copper removal
Heavy metal
Response surface method
Zeolite

A B S T R A C T

Cellulose nanocomposites were synthesized and applied to the removal of Pb(II) from aqueous solution. The synthesized nanocomposite was characterized by FT-IR, XRD, SEM, TEM, and BET analyses. Removal experiments were carried out in laboratory scale and then evaluated by response surface methodology (RSM) with a Central-Composite Design. The effects of solution pH, contact tie, initial Pb(II) concentration, adsorbent dosage and temperature on the removal efficiency were evaluated. Analysis of variance (ANOVA) was employed to find which parameter has a significant effect on the removal efficiency. The best removal efficiency value was found to be at the initial solution pH of 6.5, temperature of 34°C, initial ion concentration of 100 mg/L and the adsorbent dosage of 0.74 g/L. At this condition, the removal efficiency of Pb(II) ions was 92.54%. The adsorption equilibrium data fitted well with Langmuir isotherm model and the adsorption process followed the pseudo-second-order and intra-particle diffusion kinetic model. Thermodynamic analysis suggests that the adsorption process is endothermic, with an increasing entropy and spontaneous in nature. Besides, the nanocomposite was reused in four successive adsorption–desorption cycles, revealing a good regeneration capacity of the adsorbent. The effects of coexist cation ions on the adsorption of Pb(II) under optimal condition was also investigated. All the results demonstrate that nanocomposite is a potential recyclable adsorbent for hazardous metal ions in wastewater system.

***doi**: 10.5829/ijee.2022.13.03.06*

INTRODUCTION

The industrialization has led to an increase in the release of toxic effluents, including toxic chemicals such as heavy metals. Some of the most common heavy metals are lead, nickel, copper, mercury, chromium, cadmium, and arsenic, which are being released by dental operation, textile, tanning, electroplating, and the paper and pulp industry [1]. These heavy metals cause serious environmental problems by entering the food chain leading to severe health disorders in humans who are at the top of the food chain [2]. There is an urgent need to safeguard water and food resources from heavy metals. It has also become essential to purify water contaminated by heavy metal ions. A large number of strategies are available currently to decontaminate water to make it potable, including reverse osmosis [3] ion exchange [4, 5], cyanide treatment [6], electrochemical precipitation [7, 8], adsorption [9-16]. Most of the existing heavy metal removal technologies are limited due to their high cost. It is necessary to evolve new technologies using widely available low-cost materials for the removal of heavy metal ions [17]. Among all of these approaches, the adsorption process is considered more efficient and economical; because of its flexibility in design, simplicity of operation, facile handling, and in many cases generation of high-quality treated effluent [1]. An effective adsorbent should generally possess a high surface area, small diffusion resistance and short adsorption equilibrium time, so that it can be used to remove larger amounts of contaminants in a short period of time [18]. In addition, it should generate a minimum

*Corresponding Author Email: s.zarrinabad@protonmail.com (S.Zarinabadi)

Please cite this article as: A. Alipour, S. Zarinabadi, A. Azimi, M. Mirzaei, 2022. Effective Removal of Heavy Metal Using Cellulose Nanocomposite Adsorbents: Response Surface Methodology, Iranian (Iranica) Journal of Energy and Environment, 13(3), pp.258-272 Doi: 10.5829/ijee.2022.13.03.06

amount of sludge. Thus, developing an adsorbent with large surface area and small diffusion resistance is of great significance in practical engineering applications [19].

Compared to other host materials, porous polymeric hosts are a particularly attractive option partly because of their controllable pore size and surface chemistry as well as their excellent mechanical strength for long-term use [20]. Cellulose, a known biosorbent, is a derivative of chitin, which is the second most abundant natural polymer after cellulose [21]. Cellulose (CS) has been explored extensively for many applications; because of its low cost, hydrophilicity, biodegradability, and antimicrobial properties [22]. It has been proven to be an effective adsorbent for heavy metals; because of the amino and hydroxyl functional groups present in its structure Amine groups form complex reactions with cationic metal ions, while anionic ions are adsorbed by electrostatic attraction [23]. Despite the favorable characteristics of cellulose, it has poor mechanical strength and is unstable, which hinder its practical applications. To improve the mechanical properties of cellulose, the synthetic polymers such as poly (ethylene oxide), poly (vinyl alcohol), cellulose, and nylon-6 is blended with cellulose [17, 20]. The blends of mentioned polymers with cellulose cannot have significant effect in improving adsorption process efficiency. Therefore, the blending of cellulose with efficient material can improve the adsorption capacity of cellulose.

Recently composites of CS, like CS/cellulose composite, CS/bentonite composite, CS/fly ash composite, CS/zeolite composite, CS/cotton composite and CS/perlite composite have been created in various ways for purifying polluted water. The composites of CS/zeolite were more effective in metal ion recovery from waters and wastewaters [24].

Zeolites are one of the most universally utilized adsorbents in water treatment. Zeolites are inorganic crystalline microporous minerals (pore diameter < 2 nm) commonly used as adsorbents (purely and/or in the form of composites) [25]. They were discovered at the end of the 18th century and became commercial in 1960's when synthetic zeolites were used in various industrial filtration processes (as molecular sieves) [26] and in the crude oil [27] catalytic cracking (as catalysts). They are eco-friendly hydrated alumina silicate solids produced from the interlinked tetrahedral silica (SiO_4) and alumina (AlO_4) having several diverse crystalline structures with big open pores (occasionally called cavities) in an ordered arrangement. Certainly, as a result of their extraordinary cation-exchange capability along with their molecular sieve characteristics, zeolites are broadly used as adsorbents in purification and separation processes [28]. They are differentiated by their diverse chemical compositions, sizes and crystal structure arrangements. Their common forms are clinoptilolite, mordenite, stilbite, chabazite, analcime, laumontite and phillipsite while paulingite, offretite, mazzite and barrerite are very scarce [28]. They can act as well-organized porous solid exchange materials where the compensating cations (usually alkali metal ions) are not firmly fixed at particular sites inside the hydrated unit cell and easily exchange with cations existing within the solution [29-31]. It is noteworthy that zeolites can trap molecules within their cage-like structures. Then, molecules may be removed or exchanged without damaging the aluminosilicate framework. The zeolites structures lead to their widespread usage as adsorbents of several inorganic and organic materials [32]. The adsorption process by zeolites is dependent on many factors such as the pH, contact time, adsorbent dosage and pollutant concentration. The zeolite-A and its composites have been employed for the removal of heavy metals from water [33, 34].

The technical property of Cellulose/synthetic zeolite-A (CSZEA) composite as a potential adsorbent has not been investigated yet. The composite was characterized by using various techniques and its potential was evaluated for the removal of Pb(II). In the other part of this study, response surface methodology (RSM) based on a central composite design (CCD) has been used for the identification and optimization of the copper ions removal by synthesized nanocomposite. The experimental factors such as the amount of adsorbent, initial pH, initial ions concentration, temperature and contact time were investigated. All the parameters were simultaneously used in order to calculate their relative effects. Furthermore, the experimental data of Pb(II) removal were fitted via different isotherm and kinetic models Then, thermodynamic study of Pb(II) adsorptive removal was performed. Finally, kinetic isotherm and thermodynamics of adsorption were evaluated. The reusability of CSZEA adsorbent was examined after four cycles of adsorption-desorption processes.

MATERIAL AND METHODS

The used raw kaolinite mineral was delivered from Central Metallurgical Research & Development Institute; Iran NaOH pellets (97% purity, Alfa Aesar) were applied in the hydrothermal alteration of kaolinite into zeolite cellulose (CS) powder of deacetylation degree (MW 120,000; 85%) was applied in the production of CSZEA composites. Double distilled water was used throughout the study. Furthermore, $Cu(NO_3)_2$ were purchased from Merck company. Other chemicals were supplied by Sigma Alderich (USA).

Synthesis of zeolite-A

Zeolite-A was synthesized by the normal alkaline hydrothermal alteration of raw kaolinite. Firstly, the kaolinite was calcinated at 750°C for 4 h to produce chemically activated metakaolinite of amorphous

structure. After that, the active metakaolinite was dispersed within 100 mL of NaOH aqueous solution (3 M) at a fixed ratio of 1 metakolinite: 2 NaOH. The mixture was stirred at 500 rpm for 12 h and then, the obtained gel was set in a closed hydrothermal system of Teflon lined with stainless steel and thermally treated at 150 ℃ for 4 h. After that, the synthetic zeolite was separated from the residual solution, washed with distilled water, and dried at 70℃ for 12 h.

Synthesis of cellulose/zeolite-A composite (CSZEA)

About 4 g of the synthetic zeolite-A was homogenously dispersed within 100 mL of distilled water. The homogenization process involved stirring at 500 rpm in the existence of sonication waves at fixed power of 240 W for 180 min. After the homogenization period, the zeolite suspension was mixed with previously prepared cellulose solution (100 mL) at an adjusted stirring speed of 800 rpm and sonication irradiation of 240 W as power for 12 h. The cellulose solution was prepared by the direct dissolving of the cellulose powder (4 g) within diluted acetic acid (100 mL) of 0.1 M concentration. After the mixing interval, the composite was separated by centrifugation and washed carefully several times using distilled water to avoid the effect of the excess acetic acid. As a final step, the prepared composite was dried for 12 h at an adjusted temperature of 60 ℃ and then the powder was collected and labeled as CSZEAfor further studies.

Characterization techniques

The crystalline structures of raw kaolinite, zeolite-A, cellulose, and CSZEA composite were assessed considering their X-ray diffraction (XRD) patterns. The XRD patterns were obtaining within scanning range from 5° to 70° by X-ray diffractometer (PANalytical (Empyrean)). The functional chemical groups of zeolite-A, cellulose, CSZEAcomposite, LVOX drug, and LVOX loaded CSZEAwere addressed using Shimadzu Fourier-Transform Infrared spectrometer (FTIR−8400S) within frequency determination range from 400 to 4000 cm^{-1}. The expected changes in the morphology were followed based on the surficial images of the materials using a Scanning Electron Microscope (SEM) (Gemini, Zeiss-Ultra 55). The preparation of the samples for the SEM imaging involved coating them by thin gold layer and the imaging process was conducted after adjusting the accelerating voltage at 30 kV. The internal structure of the CSZEA composite was studied based on the obtained images using high-resolution Transmission Electron Microscope (HRTEM) (JEOL-JEM2100) after adjusting the acceleration voltage at 200 kV. The essential textural parameters of surface area, pore-volume, and pore diameter were calculated based on the N_2 adsorption/desorption isotherm curve which was obtained after treating the resulted data from a Beckman Coulter SA3100 surface area analyzer by the BJH and BET methods.

Adsorption experiments

The adsorption of copper on nanocomposite was studied by a batch technique. A certain amount of adsorbent was equilibrated with 50 mL of the heavy metals solution of known concentration in 100 mL Erlenmeyer flasks. The flasks were agitated in an incubator shaker at 150 rpm for 120 min. After that, the suspension of the adsorbent was separated from the solution by a 0.22 μm cellulosic filter. The concentration of heavy metal ions remaining in solution was measured by AAS (Perkin-Elmer 700) using the flame method. The effect of several parameters, such as pH (3-7), temperature (10-50 ºC), adsoption time (30-70 min), contaminant concentration (40-120 mg/l) and adsorbent dose (10-50 g/l) on the adsorption was investigated. The pH of the adsorptive solutions was adjusted using nitric acid (1 M) and sodium hydroxide (1 M) when needed.

Design of experiments

Response surface methodology (RSM) was used to evaluate the effects of different operating parameters on the removal efficiency of Pb(II) ions. It not only shows the optimum conditions, but it also proposes fitted regression models A 5-level, 5-factor Central Composite Design (CCD) was used to evaluate the effect of the selected parameters on the removal efficiency of Pb(II) ions from aqueous solutions by CSZEA. The four parameters affecting heavy metal removal, namely solution pH, time, temperature, initial contaminant concentration and adsorbent dosage were selected as independent variables, and the removal efficiency of Pb(II) was considered as the dependent variable (response). Variables were coded in accordance with the following equation:

$$x_i = \frac{X_i - X_0}{\Delta X_i} \quad (1)$$

where x_i is the coded value of an independent variable, X_i is the real value of an independent variable, X_0 is the real value of an independent variable at the center point and ΔX_i is the step change value. The removal efficiency of each contaminant (Y_i) was calculated according to the following equation:

$$Y(i) = \frac{C_0 - C_t}{C_0} \times 100 \quad (2)$$

where, Y is the heavy metal removal efficiency (%), and C_0 and C_t are the initial and residual concentrations of metal in solution (mg/L). The experimental range and levels of independent variables for metal ion removal were given in Table 1.

The experimental results were analyzed using Design Expert 7.0 and a regression quadratic polynomial model was proposed as follows:

$$Y = \alpha_0 + \sum_{i=1}^{k} \alpha_i x_i + \sum_{i=1}^{k} \alpha_{ii} x_{ii}^2 + \sum_{i=1}^{k} \alpha_{ij} x_i x_j + \varepsilon \quad (3)$$

Table 1. Actual and coded values of the test variables

Name	Units	Low	High	-alpha	+alpha
pH		4	6	3	7
T	min	40	60	30	70
D	g/L	0.4	0.8	0.2	1
C_0	mg/l	60	100	40	120
T	C	20	40	10	50

where, α_0 is the constant coefficient, α_i, α_{ii} and αij are the regression coefficient and X_i, X_j indicate the independent variables ε represents the random error.

RESULTS AND DISCUSSION

Characterization of the adsorbent

Structural studies

The obtained kaolinite pattern emphasizes the high crystallinity of it as a raw sample which appeared in its diffraction peaks at 12.3° (001), 20.8° (−110), 24.9° (002), and 26.6° (111) (XRD No 04-012-5104). After the transformation of kaolinite into zeolite, the obtained pattern demonstrates the detection of numerous peaks at about 7.2°, 10.32°, 12.6°, 16.2°, 21.83°, 24°, 26.2°, 27.23°, 30.1°, 30.9°, 31.1°, 32.6°, 33.39°, and 34.3° which identify the synthetic zeolite-A [32] (Figure 1B). The integrated cellulose in its single form shows the identification pattern of commercial cellulose with two observable peaks at about 9.91° and 20.22° [24] (Figure 1C).

The observed XRD pattern of CSZEA showed significant disappearance for several peaks related to the crystalline phase of the synthetic zeolite-A (Figure 1D). Moreover, the present peaks emphasize strong reduction for their diffraction intensities in addition to noticeable changes in their positions (Figure 1D). The main zeolite peaks were distinguished at 15.48°, 21.65°, 25.52°, 27.11°, and 30.6° (Figure 1D). These observations declare a successful combination between the prepared zeolite-A and the cellulose chains.

Morphological studies

The SEM and HRTEM analyses were used to detect the effect of the integration between cellulose and zeolite-A on the morphological characteristics and the internal structure of the produced composite. The SEM image of the studied raw kaolinite showed well-developed and highly crystalline pseudo-hexagonal flakey habits (Figure 2A). After the conversion process, the kaolinite flakes completely transformed into cubic crystals which distinguish the synthetic zeolite-A and confirm the synthesis of zeolite-A at high yields (Figure 2B).

After the combination of the synthetic zeolite-A with cellulose, the normal morphology of zeolite-A was changed completely and a new structure of different surficial properties was observed (Figures 2C and 2D). Generally, the zeolite cubes appeared to be completely coated with the cellulose chains which give the particles a nearly spherical shape (Figure 2C). The higher magnification revealed the presence of cellulose chains in irregular fibrous or rod-like shapes of diameter range from 50 nm to about 200 nm (Figure 2D). The intersection between the rods like cellulose particles resulted in network structure of a nanoporous matrix (Figure 2D) which will be of strong influence in improving the surface area of the final composite as compared to the essential components of zeolite-A and cellulose.

The reported morphological properties were supported by the TEM images (Figure 3). The kaolinite grains and the synthetic zeolite particles still show their pseudo-hexagonal (Figure 3A) and cubic habits, respectively (Figure 3B). The TEM images of the composite show the intersection between the rod-like cellulose particles with each other which resulted in a nanoporous polymeric matrix (Figure 3C). Additionally, the high magnification revealed the existence of the cubic zeolite-A grains as inclusion within the polymer matrix of cellulose which demonstrates strong integration between the prepared zeolite-A and the cellulose polymer as the components of the synthetic CSZEA nanocomposite (Figure 3D).

Chemical properties

The FT-IR spectra of kaolinite, zeolite-A, cellulose, and the synthetic cellulose/zeolite-a composite (A) were investigated to follow the changes in the chemical

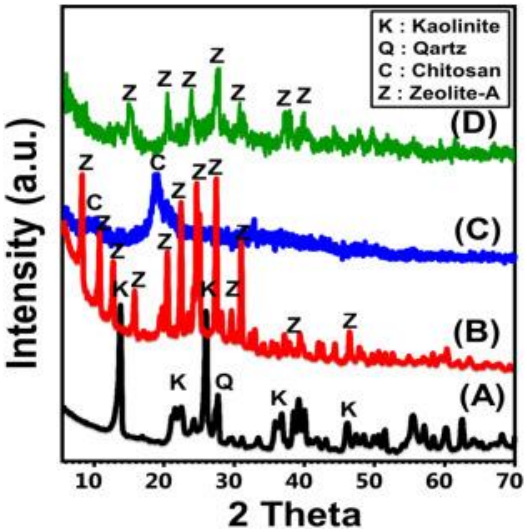

Figure 1. XRD patterns of aw kaolinite (A), synthetic zeolite-A (B), cellulose polymer (C), and the synthetic cellulose/zeolite-A composite (CH/ZA) (D)

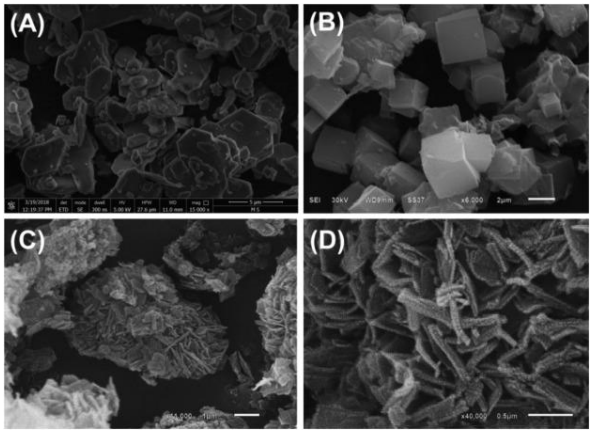

Figure 2. SEM images of raw kaolinite (A), synthetic zeolite Na- A (B), and the synthetic cellulose/zeolite-A nanocomposite (C and D)

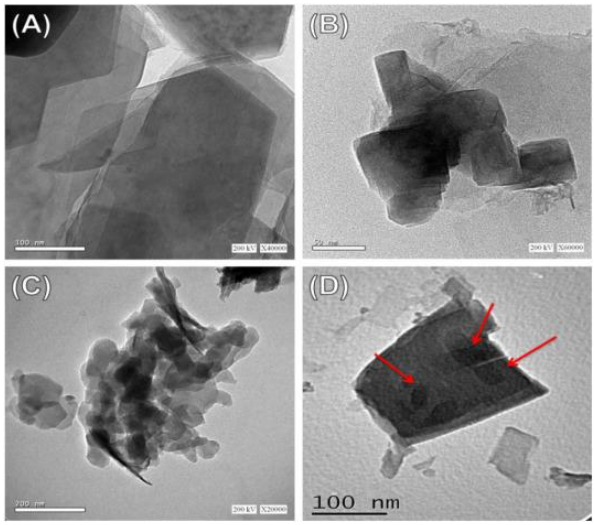

Figure 3. TEM images of raw kaolinite (A), synthetic zeolite Na-A (B), and the synthetic cellulose/zeolite-A nanocomposite (C and D) (notice, the red arrows refers to the cubes of zeolite-A within the polymer matrix)

functional groups (Figure 4). The starting kaolinite shows its distinguished spectrum with the identification bands of Si-O-Al groups at 526 cm^{-1} and 680 cm^{-1}, Si—O group at 787 cm^{-1} and 456 cm^{-1}, Si-O-Si groups at 1020 cm^{-1}, O—H bending at 1641 cm^{-1}, Al-OH groups at 3500 cm^{-1} and 912 cm^{-1}, and Si-OH groups at 3689 cm^{-1} [32] (Figure 4A).

The FT-IR spectrum of the synthetic zeolite-A shows nearly the same absorption bands of muscovite but at deviated positions. Additionally, there is noticeable disappearance for some minor bands below 1000 cm^{-1} which reflects the structural transformation of phyllosilicate kaolinite into tectosilicate zeolite (Figure 4B). The observable intensification for the OH related bands demonstrates the hydration of the kaolinite units during the alkaline transformation reactions in addition to the role of the process in etching the aluminosilicate units causing more exposure for the siloxane groups (Si-OH and Al-OH) [19, 31]. The principal bands of zeolite-A were recognized at 3612 cm^{-1} for Si-OH groups, at 3422 cm^{-1} for Al-OH groups, at 1652 cm^{-1} for the OH bending, at 990 cm^{-1} for Si-O-Si groups, at 452 cm^{-1} and 705.4 cm^{-1} for Si—O groups, and at 555 cm^{-1} as well as 630 cm^{-1} for Si-O-Al groups (Figure 4B). Moreover, a new intense band was detected at about 1475.8 cm^{-1} which identifies the characteristic coordinated water molecules within the structural channels of zeolite (Figure 4B) [33].

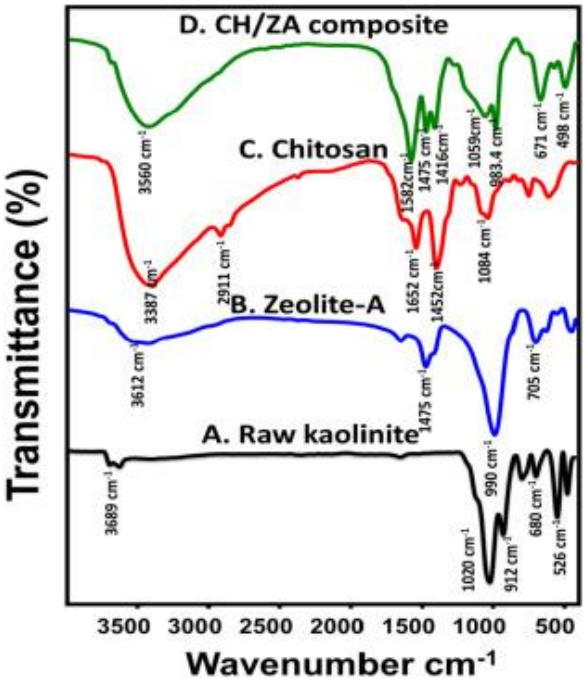

Figure 4. FT-IR spectra of raw kaolinite (A), synthetic zeolite-A (B), cellulose polymer (C), and the synthetic cellulose/zeolite-a composite (CSZEA) (D)

The inspected spectrum of cellulose polymer displays obvious bands at 1084 cm^{-1} for the functional C—O group, at 1373 cm^{-1} as well as 2911 cm^{-1} for the structural C—H, at 1452 cm^{-1} and 1653 cm^{-1} for the structural N—H group, and at 3387 cm the OH groups (Figure 4C). For the spectrum of the synthetic CSZEA composite, the identified bands are related to both cellulose and zeolite chemical groups but at shifted positions (Figure 4D). The recognized functional groups of zeolite from the spectrum of CSZEA composite are the coordinate water of zeolite-At absorption band of 1475.8 cm^{-1}, Si-O-Si group at absorption band of 983.4 cm^{-1}, Si—O group at FT-IR band of 498 cm^{-1}, and Si-O-Al groups at the absorption bands of 574cm^{-1} and 671cm^{-1} positions (Figure 4D). For cellulose as the second component of the composite, its essential chemical groups were reported at 1059.2cm^{-1} (C—O group), 1416.7cm^{-1} (C—H group), and 1582 cm^{-1} (N—H

group) (Figure 4D). The reported overlapping between the OH groups of cellulose and the OH bearing groups of zeolite resulted in a significant increase in the intensity of the identification band of this group. Such results demonstrate effective and successful integration between zeolite-A as synthetic zeolite-And the cellulose chain in a composite. The reported declination in the characteristic bands of N—H and CH groups reflected their effective role in forming the composite with the zeolite chemical group; they might be involved in chemical binding with the active siloxane groups of zeolite (Figure 4D).

Textural properties

The textural properties were evaluated considering the values of the surface area, pore-volume, and the average pore diameter for kaolinite, zeolite-A, cellulose, and CSZE Acomposite (Table 1). The conversion of kaolinite into zeolite cause increases in the surface and the pore volume The measured surface area, pore-volume, and pore diameter for zeolite-A are 423 m^2/g, 0.382 cm^3/g, and 11.6 nm, respectively while the determined values for kaolinite are 10 m^2/g, 0.072 cm^3/g, and 43.2 nm in order (Table 2). After the combination of zeolite-A and cellulose in composite (CS/ZA), the obtained surface area, pore-volume, and pore diameter increased to 446.7 m^2/g, 0.412 cm^3/g, and 23.6 nm, as compared to the measured values for zeolite-A. This might be credited to the morphological properties of the composite and the formation of the secondary nano-porous matrix as a result of the intersection between the polymer particles.

Adsorption experiments

The analysis of variance (ANOVA) is used for graphical analysis of data to obtain the interaction among the process variables and the response. The quality of the fit polynomial model is expressed by coefficient of determination (R^2). Model terms are evaluated by the P-value (probability) with 95% confidence level The analysis of variance (ANOVA) for removal efficiency (Y) is represented in Table 3. All of the response surface quadratic models for parameters in this table are significant at the 5% confidence level since the P-values are less than 0.05 The correlation coefficient (R^2) is 0.99, which it is greater than 0.80, the cut-off for a model with good fit. A high coefficient (R^2) value ensures a satisfactory adjustment of the quadratic model to the experimental data and illustrates good agreement between the calculated and observed results and shows that a desirable and reasonable agreement with the adjusted R^2. If the model terms have the P-value (probability) more than 0.05, they are considered limited influence [35]. So, they must be excluded from the study to improve the models. The model of removal efficiency is considered significant using the F-test at 5% significant level (Prob < 0.05). Insignificant model terms, which have limited influence, are excluded from the study to improve the models. Based on the results obtained, the response surface models for predicting removal efficiency is considered reasonable. The final regression model is presented in terms of its coded factors (Table 4). Model summary statistic is listed in Table 5. The pred R-squared

Table 2. The textural properties of kaolinite, zeolite-A, cellulose, and cellulose/zeolite-A nano-composite (CH/ZA)

Sample	Specific Surface area (m^2/g)	Total pore volume (cm^3/g)	Average pore size (nm)
Kaolinite	10	0.072	43.2
Zeolite-A	423	0.382	11.6
Cellulose	3.2	0.024	40.3
CSZEA composite	446.7	0.412	23.6

Table 3. ANOVA results of the regression model for optimization of Cu adsorption

Parameter	Cu		
Source	**F-value**	**p-value**	**Significance**
Model	312.60	< 0.0001	significant
A-pH	1701.06	< 0.0001	
B-t	1175.20	< 0.0001	
C-D	2562.80	< 0.0001	
D-C0	711.33	< 0.0001	
E-T	9.58	0.0043	
AB	0.4119	0.5261	
AC	4.75	0.0375	
AD	6.67	0.0151	
AE	0.0566	0.8137	
BC	5.99	0.0207	
BD	0.6837	0.4151	
BE	2.64	0.1148	
CD	0.7185	0.4036	
CE	0.2346	0.6318	
DE	0.0449	0.8337	
A^2	11.35	0.0021	
B^2	17.56	0.0002	
C^2	34.64	< 0.0001	
D^2	5.89	0.0217	
E^2	0.3064	0.5841	
Lack of Fit	8.23E-03	0.912	not significant

Table 4. The regression coefficient values

R_Cu=	+84.33
+4.26	A
+3.54	B
+5.23	C
-2.76	D
+0.3200	E
-0.0742	AB
-0.2520	AC
+0.2985	AD
+0.0275	AE
+0.2830	BC
+0.0956	BD
+0.1880	BE
+0.0980	CD
+0.0560	CE
+0.0245	DE
-0.3895	A^2
-0.4845	B^2
-0.6805	C^2
+0.2805	D^2
+0.0640	E^2

Table 5. Model summary statistic

Std. Dev.	**0.72**	R^2	**0.99**
Mean	79.97	Adjusted R^2	0.98
C.V. %	1.91	Predicted R^2	0.99
		Adeq Precision	69.93

of 0.99 was in reasonable agreement with the "adj Rsquared" of 0.98 because the difference between these values is within 0.01 which confirmed good predictability of the model. Moreover, the standard deviation for the model was 0.72 and it has been confirmed that smaller the value of standard deviation the better is the model because the predicted value obtained will be found closer to the actual value for the response. Adequate precision is a measure of the signal to noise ratio and a value greater than or equal to 4 is always desirable. In the present analysis, a value of 69.93 indicated sufficient model discrimination. On the other hand, a relatively lower value of the coefficient of variation (CV = 1.91%) indicated dependability and reproducibility of the model [35].

Predicted versus actual plot of the response was presented in Figure 5. The values predicted by the model and the results obtained by the experiments are distributed uniformly around a 45° line Normal Probability Plots for is shown in Figure 6. Normal probability plots of the studentized residuals and diagnostics are provided by Design Expert software program (a statistical software package from Stat-Ease Inc) to confirm that the selected model provides an adequate approximation of the real system Plot of Normal probability aid in evaluating the models. The normal probability plot predicts that if the residuals follow a normal distribution, as shown in Figure 6; then, the points will fall along a straight line for each case. However, some scattering is expected even with normal data; thus, the data can be considered to be normally distributed in the responses of certain model.

Response surface plots were used to determine the

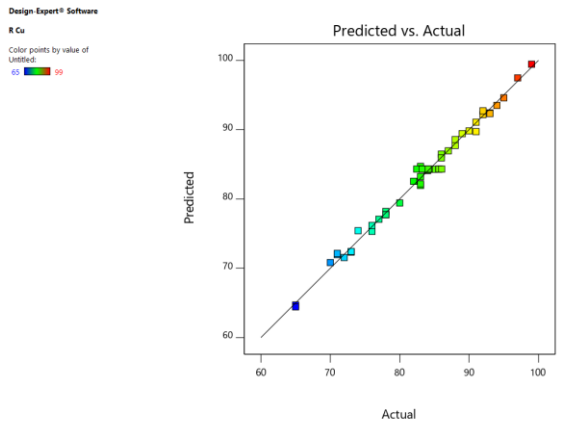

Figure 5. Predicted vs actual removal efficiency

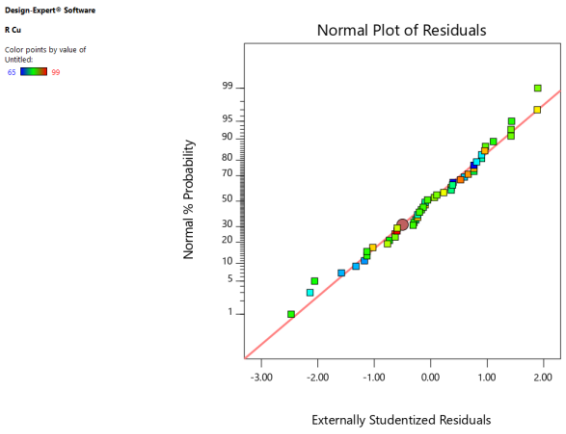

Figure 6. Normal residual plot

individual and interaction effects of the input variables on the target responses. They analyze the geometric nature of the surface, the maxima and minima of the response and the significance of the coefficients of the equation.

Sensitivity analysis

The response surface plots were obtained by varying two factors while keeping the other constant Figure 7 represents the effect of initial concentration of metals and pH on Pb(II) removal. It shows that the initial Pb(II) concentration had a negative effect on the removal efficiency of Pb(II) ions, in which by increasing the initial concentration of Pb(II) from 40 to 120 mg/L, the Pb(II) removal efficiency decreased from 89.3% to 75.4%. This behavior could be related to the complexity of competitive adsorption of the metal ions at different concentrations on the surface of the nanocomposite In the higher range of adsorbate concentration, the surface of adsorbent began to get saturated and results in decreasing the adsorption efficiency of Pb(II) ions. Copper ions needed to diffuse to the adsorbent sites by intraparticle

diffusion. In addition, steric repulsion between the copper ions could slow down the adsorption process and thereby decreases the removal rate. The solution pH is an important operational parameter in the adsorption process because it affects the solubility of the metal ions, concentration of the counter ions on the functional groups of the adsorbent and the degree of ionization of the adsorbent during reaction [31]. The adsorption efficiency increases with increasing solution pH. Electrostatic attraction is considered as the main adsorption mechanism at pH values higher than the pH_{zpc}. Metal ions can also adsorb on the surface of nanocomposite through the ion exchange process at pH values less than the pH_{zpc}. Nanocomposite pH_{zpc} was obtained around 6.7. Notably, the efficiency of adsorption increases remarkably with increasing pH value of the solution when it is below the value of 5.5 and then it increases smoothly until the pH value of 7. When the pH value is above 7, blue $Cu(OH)_2$ precipitate is formed so no adsorption experiments were conducted. The relatively lower adsorption efficiency below solution pH of 5.5 may be due to the protonation of the COO^- and NH_2 functional groups at an acidic medium. The protonated groups showed relatively lower complexation with metal ions and ion-exchange capacity, and thus the adsorption capacity was decreased.

The simultaneous influence of contact time and absorbent dosage on removal efficiency was illustrated in Figure 8. Contact time is another important parameter for adsorption efficiency of heavy metal ions. It is evidently that longer contact time is favorable for increasing the adsorption efficiency until equilibrium adsorption is established. The adsorption efficiency can reach up in a short period and then it increases mildly with extending agitation time. Such a fast adsorption rate may due to the fact that the adsorption sites are open and the metal ions interacts easily with the active sites at first and the following slower rate can be contributed to the slower diffusion of Pb(II) ions into the interior of the adsorbent during chelating process. Adsorbent dosage is another important factor which must be carefully investigated for removal process. Based on Figure 8, initially, a rapid removal of Pb(II) with an increase in adsorbent dosage was attributed to the availability of reactive sites [36]. A further increase in the nano composite dosage did not show much increase in the removal rate and adsorption equilibrium.

Figure 9 show the interaction between temperature and nanocomposite dosage Increasing temperature had a significant positive effect on the removal efficiency of Pb(II) ions The increased removal of Pb(II) ions with an increase in temperature may be a result of the faster chemical precipitation rate of copper hydroxide at the higher temperatures Higher absorbent dosage leads to higher removal efficiency This behavior could be ascribed to a greater surface area and the more availability of adsorption sites at the higher adsorbent dosage It shows that the nanoabsorbent dosage is more significant than temperature under the high concentration of CSZEA.

The interactive effects of pH and adsorbent dosage were shown in Figure 10. It shows that an increase in

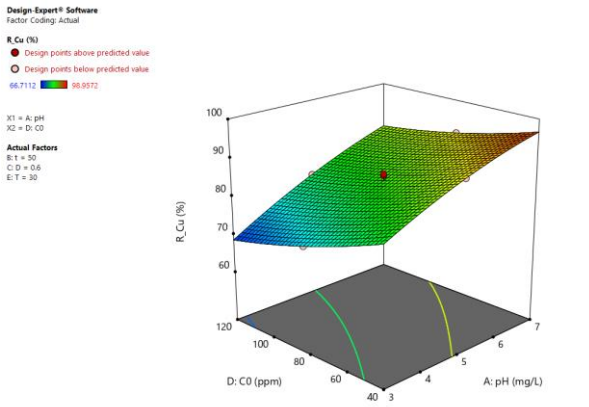

Figure 7. 3D plots for interactive effect of pH and initial Pb(II) concentration on the removal efficiency

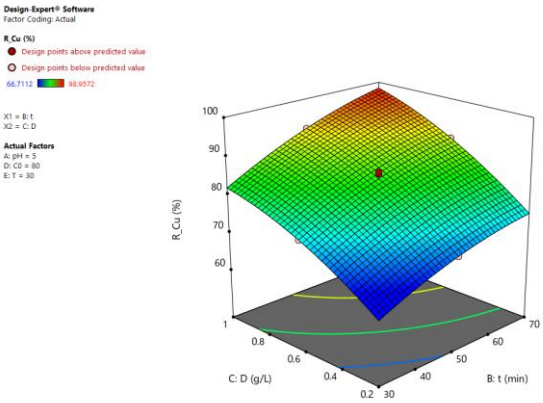

Figure 8. 3D plots for interactive effect of time and nanocomposite dosage on the removal efficiency

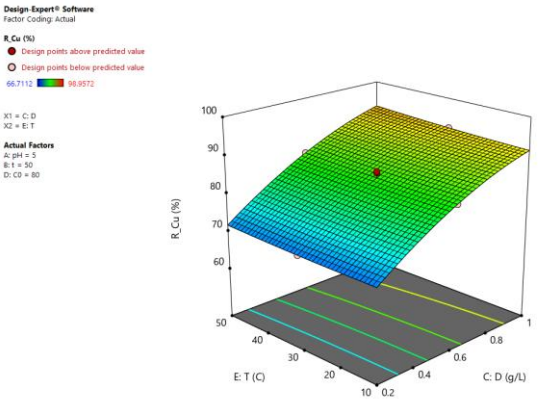

Figure 9. 3D plots for interactive effect of temperature and nanocomposite dosage on the removal efficiency

adsorbent dosage has higher effect on the adsorption of Pb(II) ions. This behavior could be ascribed to a greater surface area and the more availability of adsorption sites at the higher adsorbent dosage. Although an increase in each of pH and adsorbent dosage parameters individually had a positive effect on the removal efficiency of Pb(II) ions, the simultaneous increase of these parameters showed a negative synergistic effect on the removal.

Optimization

Maximum removal efficiency for adsorbate and the corresponding optimal conditions of variables were determined and the models were confirmed by some further experimental runs. Numerical optimization was done to find a maximum point for the desirability function by setting the values of pH, temperature, concentration of initial ions and adsorbent dosage within their ranges and maximizing the removal efficiencies of Pb(II) ions. The results listed in Table 6. The desirability value was found to be 0.93. This optimum condition was checked experimentally The results showed the removal efficiency of 90.75±1.65 for Pb(II) ions. The high degree of agreement between the predicted optimum conditions and the repeated experimental results indicated that the CCD RSM could be employed as an effective and reliable tool for evaluation and optimization of the effects of adsorption parameters on the removal efficiency of heavy metals using CSZEA nanocomposite.

Adsorption kinetic

Adsorption is a process of dynamic balance, and the adsorption rate depends on many factors such as the physical and chemical properties of adsorbent, the concentration and the characteristics of heavy metal ions and the combination ability of heavy metal ions and adsorbent. The solution was investigated at the initial metal ion concentration of 50 mg L^{-1}, the adsorbent dosage of 0.75 g/L, and pH of 6.5. Several kinetic models such as pseudo-first-order, pseudo second-order and intra-particle diffusion model have been applied to find out the adsorption mechanism. The pseudo-first-order kinetic model presumes that the binding is from physical adsorption, while the pseudo-secondorder kinetic model presumes that the binding is based on chemical adsorption.

$$log(q_t - q_e) = log\, q_e - k_1 t \quad (4)$$

$$\frac{t}{q_t} = \frac{1}{(k_2 q_e^2)} + \frac{t}{q_e} \quad (5)$$

where q_t and q_e (mmol g^{-1}) represent the amount of metal ions adsorbed on the adsorbents at time t (min) and equilibrium, respectively k_1 (min^{-1}) is the rate constant of the pseudo-first order model, while k_2 (g $mmol^{-1}$ min^{-1}) is the rate constant of pseudosecond order model.

The kinetics parameters and correlation coefficients are listed in Table 6. The higher correlation coefficients showed that the pseudo-second-order model was more applicable to describe the metal ions adsorption, implying that second order chemisorption controlled the adsorption process rather than mass transport. And the theoretical value of q_e obtained from the pseudo-second-order kinetic model was in close agreement with the experimental value.

The intraparticle diffusion model is used to explain diffusion mechanism of adsorption process [35]. The intraparticle diffusion model can be described as follows [36]:

$$q_t = k_{id} t^{0.5} + C \quad (6)$$

where K_{id} is the intraparticle diffusion rate constant (mg g^{-1} $h^{0.5}$) and C is the intercept. The value of C relates to the thickness of the boundary layer. The larger C implies the greater effect of the boundary layer [37]. Figure 11 and Table 7 show the intra-particle diffusion plots for the metal ion adsorption on CSZEA nanocomposite. It is observable that more than one linear portion appear in the plot, which indicates that the adsorption is affected by two or more steps [38]. Moreover, the diffusion rate constants in every step follow the order of $k_{i,1} > k_{i,2} > k_{i,3}$, which are

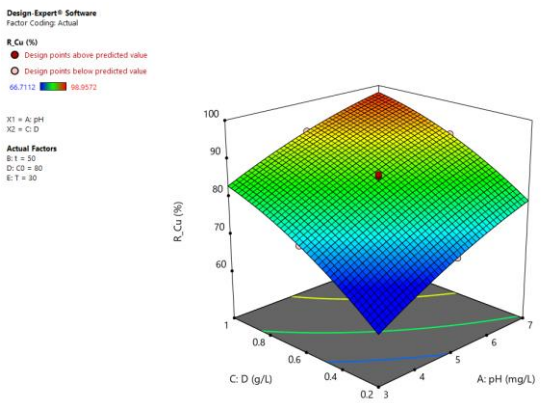

Figure 10. 3D plots for interactive effect of pH and nanocomposite dosage on the removal efficiency

Table 6. Optimization results

Parameters	Units	Values
pH		6.5
t	min	51
D	g/L	0.71
C_0	mg/l	82.5
T	C	30.3
Removal Efficiency	%	94.51

depicted in Table 6. This can be illustrated as follows: the first portion with steep slope represents the instant diffusion stage, in which large numbers of metal ions from bulk phase were adsorbed rapidly by the surface functional groups of CS/Fe_3O_4/ZnO. After almost all the exterior active points were occupied, the metal ions got ready to enter into the pores of the adsorbents [33], and then were adsorbed by the interior surface of pores, which arose in the second stage. In the third portion, the intra-particle diffusion rate constants were close to zero, indicating equilibrium state reached at last. As a summary of the kinetic studies, it is implied that both the intra-particle diffusion and the chemical chelating reaction between metal ions and active points of the adsorbents had effects on the adsorption processes [33]. Some previous kinetic studies showed similar results.

Adsorption isotherm

The adsorption isotherms could reflect the interaction pattern between adsorbent and adsorbate, further explaining the adsorption mechanisms [43]. For the adsorption isotherm studies, the tested conditions were as follows: adsorbent dosage 0.75 g/L, temperature 35°C and pH 6.5. The isotherms data of Pb(II) on nanocomposite was simulated by four well-known isotherm models, i.e, Langmuir (Equation (7)) and Freundlich (Equation (8)), Temkin (Equation (9)) and Dubinin-Radushkevich (Equation (10)) models. The Langmuir isotherm presumes that adsorption occurring on homogenous sites on the surface of adsorbents. Once the sites are occupied, adsorption cannot be achieved on the same sites. Hence, a maximum adsorption capacity is reached when all sites are occupied. The Dubinin–Radushkevich isotherm equation is more general than the Langmuir equation because it does not assume a homogeneous surface or constant adsorption potential. It was used to distinguish between the chemical and physical adsorption. The model is based on the adsorption potential theory by Polanyi Dubinin suggested that the adsorption proceeds in the volume of adsorbent micropores as opposed to layer-by-layer adsorption on micropore walls. The Freundlich isotherm is another empirical equation. It assumes that adsorbates are adsorbed to the heterogeneous surface of adsorbents, both monolayer and multilayer adsorption occur during the adsorption Temkin model accepts the following conditions: (i) the adsorption heat of all molecules present in the layer linearly decreases with the coverage which is because of adsorbent-adsorbate interactions; (ii) a uniform distribution of binding energies, up to maximum binding energy, is used to characterize the adsorption. The Temkin isotherm proposes that the decrease in the heat of adsorption is more linear rather than logarithmic as already suggested implicitly by the Freundlich equation. The isotherms curves for removal of Pb(II) by CSZEA at optimum condition were depicted in Figure 12. It is found that uptake capacities of pollutant on adsorbent raised with increasing of initial adsorbate concentration at beginning, and then reached the equilibrium.

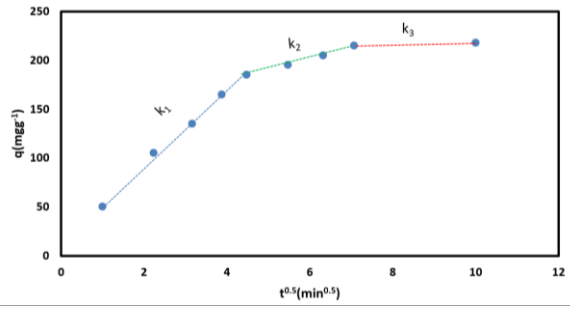

Figure 11. Intraparticle-diffusion kinetic model fits for the adsorption of Pb(II) ions on nanocomposite

Table 7. Kinetic parameters for the Pb(II) adsorption onto the nanocomposite adsorbent

Pseudo-first-order model			Pseudo-second-order model			Intra-particle diffusion model				
k_1	q_e	R^2	k_2	q_e	R^2	k_{id}			C	R^2
(min^{-1})	(mg/g)		(g/mg min)	(mg/g)		($g\ mg^{-1}\ min^{0.5}$)				
						k_1	k_2	k_3		
0.193	208.25	0.956	0.00148	228.95	0.999	53.85	13.62	0.54	1.86	0.976

The obtained values for isotherm constants and correlation coefficients are listed in Table 7. Compared with the Freundlich and Temkin isotherm models, the Langmuir model fits better with the experimental data due to the higher correlation coefficients (>0.990), which suggests a monolayer adsorption. These results indicated that adsorbent have a homogeneous surface with identical

$$q_e=(q_o K_L C_e)/(1+K_L C_e) \quad (7)$$

$$q_e= K_F(C_e)^{1/n} \quad (8)$$

$$q_e = B \ln (K_T C_e) \text{ where } B = (RT/A_T) \quad (9)$$

$$q_e =q_m \exp(-k_{DR} \varepsilon^2) \text{ where } \varepsilon=RT\ln(1+1/C_e) \quad (10)$$

where C_e (mg L^{-1}) represents concentration of pollutant in aqueous solution at equilibrium; q_e (mg g^{-1}) is adsorption amount of pollutant at equilibrium, and q_{max} (mg g^{-1}) is the maximum uptake capacity of adsorbent, respectively. K_L (L mg^{-1}) is a Langmuir constant concerning adsorption energy; n and K_F represent Freundlich constants associated with sorption intensity and sorption capacity, respectively. K_T , A_t and B_t are Temkin constant, initial adsorption heat constant (mg g^{-1}), and surface heterogeneity of the adsorbent constant (mg g^{-1}), respectively. k_{DR} is the D-R constant ($mol^2\ kJ^{-2}$) and ε shows the Polanyi potential (J mol^{-1}) R reprsent the gas constant (J $mol^{-1}\ K^{-1}$) [37].

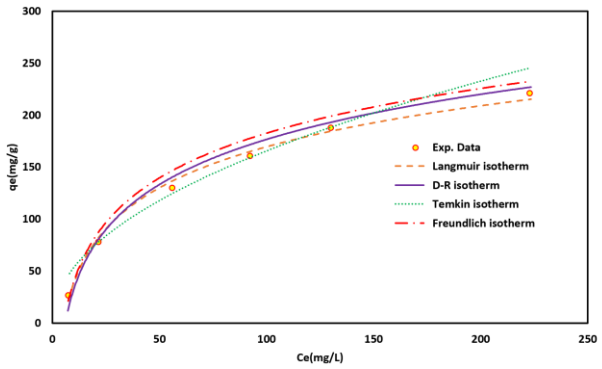

Figure 12. Isotherm models for Pb(II) adsorption by CSZEA nanocomposite

Table 8. Isotherm parameters for the Pb(II) adsorption onto the nano-composite adsorbent

	Freundlich model			Langmuir model				Temkin model			D-R model		
	n	K_F	R^2	q_m	K_L	R^2	R_L	A_T	K_T	R^2	q_m	k_{DR}	R^2
Pb(II)		(mg/g)		(mg/g)	(L/mg)			(J/mol)	(L/g)		(mg/g)	(mol^2/J^2)×10^7	
	2.362	24.65	0.901	328.46	0.0192	0.999	0.969	64.85	0.245	0.895	4.150	1.142	0.946

sorption sites. In addition, a separation factor constant (RL) was applied to evaluate the degree of suitability of dsorbent towards investigated adsorbate [45]. And the R_L is defined as follows.

$$R_L = \frac{1}{1 + K_L C_o} \quad (11)$$

where K_L (L mg^{-1}) and C_0 (mg L^{-1}) represent Langmuir constant and initial concentration of adsorbate, respectively. Thus, magnitude of R_L value represents the feasibility of adsorption. It was shown in Table 7, the values of $0 < R_L < 1$ suggests the adsorption of Pb(II) by CSZEA is favorable.

Adsorption thermodynamics

The thermodynamic parameters including Gibbs free energy change (*G*°), entropy change (*S*°) and enthalpy change (*H*°) for the adsorption of Pb(II) ions using synthesized CSZEA adsorbent were evaluated by the following equations:

$$\Delta G^\circ = -RT \ln K_L \quad (12)$$

$$\ln K_L = -\frac{\Delta H^\circ}{RT} + \frac{\Delta S^\circ}{R} \quad (13)$$

where R (8.314 J mol^{-1} K^{-1}) is the gas constant, T (K) is the absolute temperature, and K_L (L mol^{-1}) is the Langmuir constant ΔG, ΔH and ΔS are the changes in Gibbs free energy, enthalpy and entropy, respectively. After calculating equilibrium constant and related ΔG° at various temperatures, as represented in Table 8; The values of ΔH° and ΔS° which are slope and intercept of ln K_D versus 1/T plot were evaluated (Figure 13). The negative values of ΔG° confirm the spontaneous nature of the adsorption of Pb(II) on the CSZEA nanocomposite. As the temperature of the system increased, the negativity of ΔG° also increased, and proved that the temperature has a synergistic effect on the favorability. The positive value of ΔH° indicates that the adsorption reaction is endothermic. The positive value of ΔS° further confirms that the "disorder" of the system increases as a result of Pb(II) adsorption on the surface of CSZEA nanocomposite.

Results of Pb(II) ions adsorption onto cellulose-based adsorbents reported in the literature are shown in Table 9. It can be seen that the maximum adsorption capacities of CSZEA for copper ions was comparable and even higher than that of other cellulose based adsorbents except for carboxymethyl cellulose–hemicellulose resin which may be attributed to the higher specific surface area of the nanocomposite.

Regeneration of nanocomposite

Generally, the adsorbed metal ions can be desorbed and concentrated by eluant. Ethylendiamine tetraacetic acid (EDTA) is known as a very strong chelating agent for many heavy metal ions and was proposed to replace the active groups on CSZEA nanoparticles and preferentially complex with metal ions. Consequently, EDTA was chosen as the eluant for metal ions. At a concentration of 0.02 M EDTA and with the contact time of 1h, it is possible to desorb 88% of Pb(II) ions adsorbed on CSZEA into the solution Increasing EDTA concentration to 0.1 M resulted in 95% desorption of Pb(II). And the adsorption capacity of the nanoparticles could still be maintained more than 90% after four cycles.

Table 9. Thermodynamic parameters for the adsorption of Pb(II) onto the nanocomposite.

		Nanocomposite		
	T (°C)	ΔG° (kJ mol^{-1})	ΔH° (kJ mol^{-1})	ΔS° (J mol^{-1} K^{-1})
Pb(II)	15	-2.985		
	25	-4.712	12.24	124.84
	35	-5.438		

Effects of coexisting cations

The absorption capacity of Pb(II) on CSZEA nanocomposite was evaluated in presence of other metal cations (see Table 10). Also, the effect of metal cations Co^{2+}, Ni^{2+} and Pb^{2+} on the binding of copper to CSZEA has been studied in optimum condition and the results are shown in Table 11. The maximum adsorption capacity obtained for Pb(II) which was higher than the values found for Pb^{2+}, Co^{2+} and Ni^{2+}, showing the following adsorption capacity order: Pb(II) > Pb^{2+}> Co^{2+} > Ni^{2+}. These data is in agreement with the study carried out by Vold et al [38], where CS adsorbed Pb(II) selectively in the presence of Ni^{2+}, Zn^{2+}, and Cd^{2+} ions, even though no selectivity was observed for the other ions in the absence of Pb(II). Varma et al [39] reported that CS derivatives containing nitrogen as heteroatom, presented the order of affinity for divalent metal ions Pb(II) > Cd^{2+} > Ni^{2+} for Pb(II) over both Co^{2+} and Ni^{2+}. On the other hand, the higher affinity for Pb(II) than that of Co^{2+}, Ni^{2+} may be which agrees with the one observed in this study. Also, taking into account the high stability constants of Pb(II) with ammonia molecules having nitrogen atom, nanocomposite is expected as a selective chelating resin attributed to Jahn–Teller effect which is predominant for copper complexes [36]. The effect of naturally occurring interfering cations ions Na^{+}, K^{+}, Ca^{2+}, or Mg^{2+} on the binding of copper to nanocomposite was presented in Table 12 that the presence of all of the coexisting ions has little to no effect on the absorption of copper to nanocomposite. Even in extremely high amounts of cations present in solution the Pb(II) binding was still above 90%, which indicates a strong affinity of Pb(II) ions to the nanocomposite.

Table 10. Absorption capacity of Pb(II) on CSZEA nanocomposite in presence of other metal cations

	$q_{m,exp}$(mg.g^{-1})	Removal (%)
Pb(II)	328.46	91.2
Pb^{2+}	310.33	89.9
Co^{2+}	260.73	79.1
Ni^{2+}	201.38	66.7

Table 11. Interference study of copper binding to nanocomposite in the presence of Na^{+}, K^{+}, Ca^{2+}, and Mg^{2+}

	Pb(II) Removal(%)				
Concentration	**Na^{+}**	**K^{+}**	**Ca^{2+}**	**Mg^{2+}**	**All Cations**
0.3	92.20	91.86	92.52	91.89	91.80
3	92.06	91.52	93.05	91.30	90.25
30	91.41	92.34	92.14	92.41	92.14
300	91.10	92.41	91.85	90.86	89.64

Table 12. Comparison of adsorption capacities of various cellulose-based adsorbents for Pb(II) ions

Adsorbent	Adsorption condition	q_m	Isotherm	Kinetic	Thermodynamic	References
Raw cellulose	25°C, pH 5.5	80.17	Langmuir	Pseudo-second-order		[40]
Magnetic cellulose microcapsules	pH 7.0, 30°C	104	Langmuir	Pseudo-second-order		[41]
Epichlorohydrin cross-linked xanthate cellulose	pH 5.0, 30°C	43.47	Langmuir	Pseudo-second-order	endothermic	[42]
Magnetic cellulose nanoparticles	pH 5.0, 35°C	35.5	Langmuir			[43]
Xanthate-modified magnetic cellulose	25°C, pH 5.0	34.5	Langmuir			[44]
Magnetic cellulose modified by melamine	25°C, pH 5.0	163.9	Langmuir			[45]
S-doped Fe_3O_4@cellulose		46.6	Freundlich			[46]
EDTA-modified cellulose/SiO_2/Fe_3O_4	25°C, pH 5.0	31.4	Langmuir	Pseudo-second-order	endothermic	[36]
Cellulose coated cotton fiber	25°C, pH 6.5	18.08	Langmuir			[47]
Porous cellulose-oxalate	30°C, pH 5.0	227.27	Langmuir	Pseudo-second-order	endothermic	[48]
Non-porous cellulose-oxalate	30°C, pH 5.0	175.44	Langmuir	Pseudo-second-order	endothermic	[48]
Thiourea-modified magnetic cellulose microspheres	28°C, pH 5.0	66.7	Langmuir	Pseudo-second-order		[49]

Magnetic cellulose/cellulose microsphere	30°C	88.21	Langmuir			[50]
Cellulose-modified $MnFe_2O_4$	pH 6.5	65.1	Langmuir			[51]
Magnetic cellulose nanoparticles	pH 5.0, 25°C	33.7	Langmuir	Pseudo-second-order		[43]
Cellulose/poly(acrylic acid) magnetic	pH 5.5, 30°C	174.0	Langmuir	Pseudo-second-order		[52]
Magnetic cellulose	pH 5.5, 25°C	216.6	Langmuir	Pseudo-second-order	endothermic	[53]
Magnetic cellulose bead	pH 4.0, 30°C	147.0	Langmuir			[21]
Carboxymethyl cellulose–hemicellulose resin	pH 4.0, 25°C	333.3	Langmuir	Pseudo-second-order		[54]
Fe_3O_4-CS/EDTA	pH 3.0, 30°C	225	Langmuir	Pseudo-second-order	endothermic	[55]
CSZEA	pH 6.5, 34°C	328.46	Langmuir	Pseudo-second-order/ Intraparticle diffusion	endothermic	Present study

CONCLUSION

In this research, a novel CSZEA nanocomposite was used to remove Pb(II) ions from aqueous solution Nanocomposite was synthesized and characterized by XRD, FTIR, BET, SEM, TEM, analyses Response surface methodology was used to find a maximum location in the design space for removal process A Central Composite Design was employed to evaluate the effects of pH, temperature, initial contaminant concentration, contact time and adsorbent dosage on the removal efficiency of Pb(II) ions on nanocomposite under competitive conditions Quadratic models were well fitted to the experimental data and second-order polynomial equations (regression models) were described the relationship between the responses and the variables accurately The corresponding optimal conditions of variables of adsorption process were determined to be at the pH of 6.5, contact time of 56 min, the temperature of 34°C, the initial metal concentration of 100 mg/L (each metal ion) and the adsorbent dosage of 0.75 g/L Kinetic studies indicated that the adsorption reaction follows pseudo-second order kinetics, suggesting the main adsorption mechanism of chemical adsorption The equilibrium data could be described by the Langmuir isotherms The adsorbent possesses excellent regenerative performance.

REFERENCES

1. Kim, S., Chu, K. H., Al-Hamadani, Y. A., Park, C. M., Jang, M., Kim, D.-H., Yu, M., Heo, J. and Yoon, Y., 2017. Removal of contaminants of emerging concern by membranes in water and wastewater: A review, *Chemical Engineering Journal*, 335, pp. 896-914. Doi: 10.1016/j.cej.2017.11.044
2. Fu, F. and Wang, Q., 2011. Removal of heavy metal ions from wastewaters: A review, *Journal of Environmental Management*, 92(3), pp. 407-418. Doi:10.1016/j.jenvman.2010.11.011
3. Lee, K. P., C.Arnot, T. and Mattia, D., 2011. A review of reverse osmosis membrane materials for desalination—Development to date and future potential, *Journal of Membrane Science*, 370(1–2), pp. 1-22.
4. Wan, S., Zhao, X., Lv, L., Su, Q., Gu, H., Pan, B., Zhang, W., Lin, Z. and Luan, J., 2010. Selective adsorption of Cd(II) and Zn(II) ions by nano-hydrous manganese dioxide (HMO)-encapsulated cation exchanger, *Industrial and Engineering Chemistry Research*, 49(16), pp. 7574-7579. Doi:10.1021/ie101003y
5. Bai, Y. and Bartkiewicz, B., 2009. Removal of Cadmium from Wastewater Using Ion Exchange Resin Amberjet 1200H Columns, *Polish Journal of Environmental Studies*, 18(6), pp. 1191–1195.
6. Wild, S. R., Rudd, T. and Neller, A., 1994. Fate and effects of cyanide during wastewater treatment processes, *Science of The Total Environment*, 156(2), pp. 93-107. Doi: 10.1016/0048-9697(94)90346-8
7. Cao, B., Teng, X., Heo, S. H., Li, Y., Cho, S. O., Li, G. and Cai, W., 2007. Different ZnO nanostructures fabricated by a seed-layer assisted electrochemical route and their photoluminescence and field emission properties, *Journal of Physical Chemistry C*, 111(6), pp. 2470-2476. Doi:10.1021/jp066661l
8. Cao, B., Cai, W., Zeng, H. and Duan, G., 2006. Morphology evolution and photoluminescence properties of ZnO films electrochemically deposited on conductive glass substrates, *Journal of Applied Physics*, 99(7). Doi:10.1063/1.2188132
9. Zhu, K., Duan, Y., Wang, F., Gao, P., Jia, H., Ma, C. and Wang, C., 2017. Silane-modified halloysite/Fe_3O_4 nanocomposites: Simultaneous removal of Cr (VI) and Sb (V) and positive effects of Cr (VI) on Sb (V) adsorption, *Chemical Engineering Journal*, 311, pp. 236-246.
10. Xu, Q., Wang, Y., Jin, L., Wang, Y. and Qin, M., 2017. Adsorption of Cu (II), Pb (II) and Cr (VI) from aqueous solutions using black wattle tannin-immobilized nanocellulose, *Journal of hazardous materials*, 339, pp. 91-99. Doi: 10.1016/j.jhazmat.2017.06.005
11. Sun, J., Wang, C., Zeng, L., Xu, P., Yang, X., Chen, J., Xing, X., Jin, Q. and Yu, R., 2016. Controllable assembly of CeO2 micro/nanospheres with adjustable size and their application in Cr (VI) adsorption, *Materials Research Bulletin*, 75, pp. 110-114. Doi: 10.1016/j.materresbull.2015.11.035
12. Ren, H., Jiang, J., Wu, D., Gao, Z., Sun, Y. and Luo, C., 2016. Selective adsorption of Pb (II) and Cr (VI) by surfactant-modified

and unmodified natural zeolites: a comparative study on kinetics, equilibrium, and mechanism, *Water, Air, & Soil Pollution*, 227(4), pp. 101. Doi: 10.1007/s11270-016-2790-6
13. Li, X., Gao, X., Ai, L. and Jiang, J., 2015. Mechanistic insight into the interaction and adsorption of Cr (VI) with zeolitic imidazolate framework-67 microcrystals from aqueous solution, *Chemical Engineering Journal*, 274, pp. 238-246. Doi: 10.1016/j.cej.2015.03.127
14. Yari, S., Abbasizadeh, S., Mousavi, S. E., Moghaddam, M. S. and Moghaddam, A. Z., 2015. Adsorption of Pb (II) and Cu (II) ions from aqueous solution by an electrospun CeO_2 nanofiber adsorbent functionalized with mercapto groups, *Process Safety and Environmental Protection*, 94, pp. 159-171. Doi: 10.1016/j.psep.2015.01.011
15. Liu, W., Zhang, J., Jin, Y., Zhao, X. and Cai, Z., 2015. Adsorption of Pb (II), Cd (II) and Zn (II) by extracellular polymeric substances extracted from aerobic granular sludge: efficiency of protein, *Journal of Environmental Chemical Engineering*, 3(2), pp. 1223-1232. Doi: 10.1016/j.jece.2015.04.009
16. Cao, C., Xiao, L., Chen, C., Shi, X., Cao, Q. and Gao, L., 2014. In situ preparation of magnetic Fe_3O_4/chitosan nanoparticles via a novel reduction–precipitation method and their application in adsorption of reactive azo dye, *Powder Technology*, 260, pp. 90-97. Doi: 10.1016/j.powtec.2014.03.025
17. Malathi, S., Daniel, S. C. G. K., Vaishnavi, S., Sivakumar, M. and Balasubramanian, S., 2014. Chitosan-based polymer nanocomposites for heavy metal removal (Chapter 1), *Nanocomposites in Wastewater Treatment*, Pan Stanford Publishing Pte. Ltd., pp.1-22. eISSN: 978-981-4463-55-3
18. Ahmadi, A., Heidarzadeh, S., Mokhtari, A. R., Darezereshki, E. and AsadiHarouni, H., 2014. Optimization of heavy metal removal from aqueous solutions by maghemite (γ-Fe_2O_3) nanoparticles using response surface methodology, *Journal of Geochemical Exploration*, 147, pp. 151-158. Doi: 10.1016/j.gexplo.2014.10.005
19. Radoń, A., Drygała, A., Hawełek, Ł. and Łukowiec, D., 2017. Structure and optical properties of Fe_3O_4 nanoparticles synthesized by co-precipitation method with different organic modifiers, *Materials Characterization* 131, pp. 148-156. Doi: 10.1016/j.matchar.2017.06.034
20. Sureshkumar, V., Daniel, S. K., Ruckmani, K. and Sivakumar, M., 2016. Fabrication of chitosan–magnetite nanocomposite strip for chromium removal, *Applied Nanoscience*, 6(2), pp. 277-285. Doi: 10.1007/s13204-015-0429-3
21. Fan, C., Li, K., He, Y., Wang, Y., Qian, X. and Ji, J., 2018. Evaluation of magnetic chitosan beads for adsorption of heavy metal ions, *Science of The Total Environment*, 627, pp. 1396-1403. Doi: 10.1016/j.scitotenv.2018.02.033
22. Song, X., Li, L., Zhou, L. and Chen, P., 2018. Magnetic thiolated/quaternized-chitosan composites design and application for various heavy metal ions removal, including cation and anion, *Chemical Engineering Research and Design*, 136, pp. 581-592. Doi: 10.1016/j.cherd.2018.06.025
23. Rathinam, K., Singh, S. P., Arnusch, C. J. and Kasher, R., 2018. An environmentally-friendly chitosan-lysozyme biocomposite for the effective removal of dyes and heavy metals from aqueous solutions, *Carbohydrate Polymers*, 199, pp. 506-515. Doi: 10.1016/j.carbpol.2018.07.055
24. Yu, J. and Wang, D., 2021. Current trends and challenges in the synthesis and applications of chitosan-based nanocomposites for plants: A review, *Carbohydrate Polymers*, 261, pp. 117904. Doi: 10.1016/j.carbpol.2021.117904
25. Zayed, A. M., Selim, A. Q., Mohamed, E. A., Abdel Wahed, M. S. M., Seliem, M. K. and Sillanpää, M., 2017. Adsorption characteristics of Na-A zeolites synthesized from Egyptian kaolinite for manganese in aqueous solutions: Response surface modeling and optimization, *Applied Clay Science*, 140, pp. 17-24. Doi:10.1016/j.clay.2017.01.027
26. Bessa, R. D. A., Costa, L. D. S., Oliveira, C. P., Bohn, F., do Nascimento, R. F., Sasaki, J. M. and Loiola, A. R., 2017. Kaolin-based magnetic zeolites A and P as water softeners, *Microporous and Mesoporous Materials*, 245, pp. 64-72. Doi:10.1016/j.micromeso.2017.03.004
27. Zeng, P., Guo, X., Zhu, X., Guo, Q., Wang, Y., Ren, S. and Shen, B., 2017. On the synthesis and catalytic cracking properties of Al-ITQ-13 zeolites, *Microporous and Mesoporous Materials*, 246, pp. 186-192. Doi:10.1016/j.micromeso.2017.03.033
28. Akhigbe, L., Ouki, S. and Saroj, D., 2016. Disinfection and removal performance for Escherichia coli and heavy metals by silver-modified zeolite in a fixed bed column, *Chemical Engineering Journal*, 295, pp. 92-98. Doi:10.1016/j.cej.2016.03.020
29. Visa, M., 2016. Synthesis and characterization of new zeolite materials obtained from fly ash for heavy metals removal in advanced wastewater treatment, *Powder Technology*, 294, pp. 338-347. Doi:10.1016/j.powtec.2016.02.019
30. Irani, M., Amjadi, M. and Mousavian, M. A., 2011. Comparative study of lead sorption onto natural perlite, dolomite and diatomite, *Chemical Engineering Journal*, 178, pp. 317-323. Doi:10.1016/j.cej.2011.10.011
31. Wang, S. and Peng, Y., 2010. Natural zeolites as effective adsorbents in water and wastewater treatment, *Chemical Engineering Journal*, 156(1), pp. 11-24. Doi:10.1016/j.cej.2009.10.029
32. Yurekli, Y., 2016. Removal of heavy metals in wastewater by using zeolite nano-particles impregnated polysulfone membranes, *Journal of Hazardous Materials*, 309, pp. 53-64. Doi:10.1016/j.jhazmat.2016.01.064
33. Braschi, I., Blasioli, S., Buscaroli, E., Montecchio, D. and Martucci, A., 2016. Physicochemical regeneration of high silica zeolite Y used to clean-up water polluted with sulfonamide antibiotics, *Journal of Environmental Sciences (China)*, 43, pp. 302-312. Doi:10.1016/j.jes.2015.07.017
34. El-Mekkawi, D. M. and Selim, M. M., 2014. Removal of Pb^{2+} from water by using Na-Y zeolites prepared from Egyptian kaolins collected from different sources, *Journal of Environmental Chemical Engineering*, 2(1), pp. 723-730. Doi:10.1016/j.jece.2013.11.014
35. Alizadeh, M. and Sadrameli, S. M., 2018. Numerical modeling and optimization of thermal comfort in building: Central composite design and CFD Simulation, *Energy and Buildings*, 164, pp. 187-202. Doi: 10.1016/j.enbuild.2018.01.006
36. Ren, Y., Abbood, H. A., He, F., Peng, H. and Huang, K., 2013. Magnetic EDTA-modified chitosan/SiO_2/Fe_3O_4 adsorbent: Preparation, characterization, and application in heavy metal adsorption, *Chemical Engineering Journal*, 226, pp. 300-311. Doi: 10.1016/j.cej.2013.04.059
37. Kulkarni, S., Dhokpande, S. and Kaware, J., 2014. A Review on Isotherms and Kinetics of Heavy Metal Removal, *International Journal of Ethics in Engineering & Management Education*, 1(2). https://www.academia.edu/download/33280636/FEB-1-_4-_A_Review_on_Isotherms_and_Kinetics_of_Heavy_Metal_Removal.pdf
38. Vold, I. M. N., Varum, K. M., Guibal, E. and Smidsrod, O., 2003. Binding of ions to chitosan—selectivity studies, *Carbohydr. Polym.*, 54 pp. 471. Doi: 10.1016/j.carbpol.2003.07.001
39. Varma, A. J., Deshpande, S. V. and Kennedy, J. F., 2004. Metal complexation by chitosan and its derivatives: a review, *Carbohydrate Polymers*, 55, pp. 77-93. Doi: 10.1016/j.carbpol.2003.08.005
40. Ngah, W. S. W., Endud, C. S. and Mayanar, R., 2002. Removal of copper(II) ions from aqueous solution onto chitosan and cross-linked chitosan beads, *Reactive & Functional Polymers*, 50, pp. 181-190.
41. Zhang, S., Zhou, Y., Nie, W., Song, L. and Zhang, T., 2012. Preparation of uniform magnetic chitosan microcapsules and their application in adsorbing copper ion(II) and chromium Ion(III), *Industrial & Engineering Chemistry Research.*, 51, pp. 14099-14106.
42. Kannamba, B., Reddy, K. L. and AppaRao, B. V., 2010. Removal of Cu(II) from aqueous solutions using chemically modified

chitosan, *Journal of Hazardous Materials*, 175, pp. 939-948. Doi: 10.1016/j.jhazmat.2009.10.098
43. Chen, Y. and Wang, J., 2011. Preparation and characterization of magnetic chitosan nanoparticles and its application for Cu(II) removal, *Chemical Engineering Journal*, 168, pp. 286-292. Doi: 10.1016/j.cej.2011.01.006
44. Zhu, Y. H., Hu, J. and Wang, J. L., 2012. Competitive adsorption of Pb(II), Cu (II) and Zn (II) onto xanthate-modified magnetic chitosan, *Journal of Hazardous Materials*, 221–222, pp. 155-161. Doi: 10.1016/j.jhazmat.2012.04.026
45. Wu, Z.-C., Wang, Z.-Z., Liu, J., Yin, J.-H. and Kuang, S.-P., 2015. A new porous magnetic chitosan modified by melamine for fast and efficient adsorption of Cu (II) ions, *International Journal of Biological Macromolecules*, 81, pp. 838-846. Doi: 10.1016/j.ijbiomac.2015.09.020
46. Zhao, L. Q., Chang, X. L., Liao, R., Zhang, X. L., Xie, J. R., Yu, B. W., Wu, R. H., Wan, R. J. and Yang, S. T., 2014. Facile hydrothermal preparation of S-doped Fe_3O_4@C nanoparticles for Cu^{2+} removal, *Materials Letters*, 135 pp. 154-157. Doi: 10.1016/j.matlet.2014.07.166
47. Zhang, G., Qu, R., Sun, C., Ji, C., Chen, H., Wang, C. and Niu, Y., 2008. Adsorption for metal ions of chitosan coated cotton fiber, *Journal of Applied Polymer Science*, 110, pp. 2321-2327. Doi: 10.1002/app.27515
48. Mi, F.-L., Wu, S.-J. and Lin, F.-M., 2015. Adsorption of copper (II) ions by a chitosan-oxalate complex biosorbent, *International Journal of Biological Macromolecules*, 72, pp. 136-144.
49. Zhou, L. M., Wang, Y. P., Liu, Z. R. and Huang, Q. W., 2009. Characteristics of equilibrium, kinetics studies for adsorption of Hg(II), Cu(II), and Ni(II) ions by thiourea-modified magnetic chitosan microspheres, *Journal of Hazardous Materials*, 161, pp. 995-1002. Doi: 10.1016/j.jhazmat.2008.04.078
50. Luo, X. G., Zeng, J., Liu, S. L. and Zhang, L. N., 2015. An effective and recyclable adsorbent for the removal of heavy metal ions from aqueous system: magnetic chitosan/cellulose microspheres, *Bioresoure Technology*, 194, pp. 403-406. Doi: 10.1016/j.biortech.2015.07.044
51. Meng, Y. Y., Chen, D. Y., Sun, Y. T., Jiao, D. L., Zeng, D. C. and Liu, Z. W., 2015. Adsorption of Cu^{2+} ions using chitosan-modified magnetic Mn ferrite nanoparticles synthesized by microwave-assisted hydrothermal method, *Applied Surface Science*, 324, pp.745-750. Doi: 10.1016/j.apsusc.2014.11.028
52. Yan, H., Yang, L., Yang, Z., Yang, H., Lia, A. and Cheng, R., 2012. Preparation of chitosan/poly(acrylic acid) magnetic composite microspheres and applications in the removal of copper(II) ions from aqueous solutions, *Journal of Hazardous Material*, 229–230, pp. 371-380. Doi: 10.1016/j.jhazmat.2012.06.014
53. Li, J., Jiang, B., Liu, Y., Qiu, C., Hu, J., Qian, G., Guo, W. and Ngo, H. H., 2017. Preparation and adsorption properties of magnetic chitosan composite adsorbent for Cu^{2+} removal, *Journal of Cleaner Production*, 158, pp. 51-58. Doi: 10.1016/j.jclepro.2017.04.156
54. Wu, S.-P., Dai, X.-Z., Kan, J.-R., Shilong, F.-D. and Zhu, M.-Y., 2017. Fabrication of carboxymethyl chitosan–hemicellulose resin for adsorptive removal of heavy metals from wastewater, *Chinese Chemical Letters*, 28, pp. 625–632. Doi: 10.1016/j.cclet.2016.11.015
55. Chen, B., Zhao, H. and Chen, S., 2019. A magnetically recyclable chitosan composite adsorbent functionalized with EDTA for simultaneous capture of anionic dye and heavy metals in complex wastewater, *Chemical Engineering Journal*, 356, pp. 69-80. Doi: 10.1016/j.cej.2018.08.222

Persian Abstract

چکیده

نانوکامپوزیت های سلولزی سنتز و برای حذف سرب (II) از محلول آبی مورد استفاده قرار گرفتند. نانوکامپوزیت سنتزشده توسط آنالیزهای FT-IR، XRD، SEM، TEM و BET مشخص شده و مورد مطالعه قرار گرفتند. آزمایش‌های حذف فلز در مقیاس آزمایشگاهی انجام گردید و سپس با روش پاسخ سطح (RSM) با طرح مرکب مرکزی ارزیابی شد. اثرات pH محلول، پیوند تماس، غلظت اولیه سرب(II)، دُز جاذب و دما بر راندمان حذف مورد ارزیابی قرار گرفت. از آنالیز واریانس (ANOVA) برای یافتن اینکه کدام پارامتر بر راندمان حذف اثر قابل توجهی دارد، استفاده شد. بهترین مقدار بازدهی حذف یون سرب (II) در شرایطی که pH محلول اولیه ۶/۵، دمای ۳۴ درجه سانتی‌گراد، غلظت اولیه یون ۱۰۰ میلی‌گرم در لیتر و دُز جاذب ۰/۷۴ گرم در لیتر بوده است، ۹۲/۵۴ درصد بدست آمد. داده‌های تعادل جذب به خوبی با مدل ایزوترم لانگمویر برازش داده شد و فرآیند جذب از مدل سینتیکی شبه مرتبه دوم و انتشار درون ذره پیروی کرد. تجزیه و تحلیل ترمودینامیکی نشان می‌دهد که فرآیند جذب گرماگیر و با آنتروپی فزاینده بوده و ماهیت خود به خودی دارد. علاوه بر این نانوکامپوزیت در چهار چرخه جذب-واجذب متوالی مورد استفاده مجدد قرار گرفت و ظرفیت بازسازی خوبی از جاذب را نشان داد. اثرات همزیستی یون‌های کاتیون بر جذب سرب (II) در شرایط بهینه نیز مورد بررسی قرار گرفت. کلیه نتایج نشان دادند که نانوکامپوزیت یک جاذب بالقوه قابل بازیافت برای یون‌های فلزی خطرناک در سیستم فاضلاب می‌باشد.